Three-Dimensional Turbulent Structure and Associated

Secondary Currents in Straight Rivers

—— Field Measurements of River Turbulence ——

by

Iehisa Nezu*, Akihiro Tominaga** and Hiroji Nakagawa***

(Received June 23, 1992)

Abstract

Fundamental structures of turbulence in two-dimensional (2-D) and further three-dimensional (3-D) open-channel flows have recently been almost clarified theoretically and experimentally through accurate experimental data which were obtained using a laser-Doppler anemometer system in laboratory flumes; this detailed knowledge is now available in an IAHR monograph written by Nezu & Nakagawa (1992). Many of these experiments have, however, been conducted at moderate Reynolds numbers, say $Re \simeq 10^4$. Therefore, it is not yet clear whether such laboratory data of open-channel turbulence can be applied to river turbulence at high Reynolds numbers. In this study, velocity measurements of the Biwako-Sosui River ($Re = 8 \times 10^5$) in Kyoto and the Aichi Irrigation Channel ($Re = 6 \times 10^5$) in Nagoya have been conducted, using three-component electromagnetic flow meters. It was first found that multi-cellular secondary currents and free-surface secondary currents were evident in actual rivers. The features of such secondary currents in rivers were in a good agreement with those in laboratory flumes.

Key Words: *turbulence-driven secondary currents*; *river turbulence*; *field measurements*; *velocity-dip phenomenon*; *effects of aspect ratio*.

1. Introduction

Velocity measurements in rivers have already been carried out for more than about 100 years. As far as the authors know, Stearns (1883) in the USA and Möller (1883) in Germany independently measured the velocity distributions in rivers and discovered that the maximum velocity appeared below the water surface in a narrow river. Gibson (1909) also found the same velocity-dip phenomenon in the field streams of England. As the reason for such a velocity-dip phenomenon, all of them presumed the existence of a pair

---

* Assoc. Professor, Division of Global Environment Engineering, Graduate School of Engineering, Kyoto University, Kyoto 606, Japan.
** Assoc. Professor, Department of Civil Engineering, Nagoya Institute of Technology, Nagoya 466.
*** Dean, Professor, Division of Global Environment Engineering, Graduate School of Engineering, Kyoto University, Kyoto 606.

of secondary currents in streams; these currents flow from the bank towards the center along the free surface and turn downwards at the center of the channel.

Fluvial flows in wide channels are important in the field of river engineering. Vanoni (1946) pointed out that the spanwise distribution of sediment concentration varied periodically in wide open channels, and he inferred that this phenomenon might either generate or be generated by cellular secondary currents. Kinoshita (1967) discovered through an aerial stereoscopic photo-survey of rivers in flood in Japan that low-speed zones of the water-surface velocity, associated with boils of high sediment, appeared with the spanwise spacing of twice the flow depth, h, and that the corresponding high-speed zones appeared on both sides of the low-speed zones. He suggested then that there might exist multi-cellular secondary currents in straight wide rivers which had a pair of counter rotating longitudinal vortices with a vortex diameter of about h. The existence of multi-cellular secondary currents has also been suggested from observations of three-dimensional bed configurations such as longitudinal ridges and troughs on the river bed (e.g., Karcz [1966], Culbertson [1967] and Allen [1985]).

The above-mentioned three-dimensional (3-D) flow structures associated with secondary currents have not been verified quantitatively by field measurements due to the poor measuring accuracy of instruments; the velocity of secondary currents is within only a few percentage points of main flow velocity. Furthermore, it is necessary to conduct direct measurements of turbulence in order to investigate the generation mechanism of secondary currents in straight channels because they are generated by anisotropy of turbulence.

Fortunately, accurate turbulence measurements in laboratory flumes have become feasible in the last ten years with a refined hot-film anemometer and recently developed laser Doppler anemometer (LDA). Nezu & Rodi (1985) and Nezu et al. (1989) have conducted accurate measurements of secondary currents in straight rectangular open-channel flows, by making use of a two-component LDA system. They found a significant difference between the turbulence-driven secondary currents in duct flows and open-channel flows. The secondary currents are generated in open-channel flows, due to the anisotropy of turbulence near the free surface because the vertical component of turbulence is much more depressed near the free surface in open channels than in ducts. It has then been proved that the maximum velocity appeared below the free surface due to the existence of secondary currents. These important characteristics of secondary currents peculiar to rectangular open-channel flows were also computer-simulated reasonably by Naot & Rodi (1982) using an algebraic stress model of turbulence.

Furthermore, the cross section of rivers is often trapezoidal. So, Tominaga et al. (1989) tried to conduct some refined hot-film measurements in trapezoidal open-channel flows; the angle θ of the trapezoid to the horizontal axis was systematically varied; $\theta = 32°$, $44°$ and $60°$. They found that the dip in the maximum velocity position did not appear in

trapezoidal open channels.

Many laboratory experiments and numerical calculations have been conducted at moderate Reynolds numbers, say Re $\simeq 10^4$, and fundamental knowledge about 2-D and 3-D turbulent structures of open-channel flows are now available (e.g., an IAHR-monograph written by Nezu & Nakagawa [1992]).   However, it is not yet clear whether these laboratory data of open-channel turbulence can be applied to river turbulence at high Reynolds numbers.   In this study, turbulence measurements of both the Biwako-Sosui urban river in Kyoto and the Aichi irrigation channel in Nagoya have been conducted using three-component electromagnetic flow meters.   The former represented a wide open-channel flow in which multi-cellular secondary currents appeared evident.   On the other hand, the latter represented a narrow open-channel flow in which free-surface secondary currents were generated predominantly.   These features of secondary currents in rivers coincided well with those observed in laboratory experiments.

2. Review of Turbulence Measurements in Rivers and Estuaries

Table 1 indicates the main examples of turbulence measurements conducted in rivers and estuaries.   Some splendid research that contributed greatly to the hydraulics and fluid mechanics fields are included in Table 1.   Grant *et al.* (1962) conducted some turbulence measurements in a tidal channel on the west coast of Canada by making use of a hand-made conical-type hot-film probe.   Since the Reynolds number was as large as Re $\simeq 10^8$, they could verify the validity of Kolmogoroff's $-5/3$ power law in the one-dimensional spectra; the inertial subrange of $-5/3$ power law becomes wider with an increase of the Reynolds number.   Consequently, the Kolmogoroff constant C was reasonably determined from these experiments, i.e., $C = 0.47$, and since then this experimental value has been used often to evaluate the turbulent dissipation ε in both laboratory and field flows.

Another notable study is the discovery of bursting phenomena in rivers and estuaries by Gordon (1974) and Heathershaw (1974).   These phenomena were first discovered in a laboratory water channel by flow visualization.   The investigation of Grant *et al.* is based on a classical statistical theory of turbulence, whereas that of Gordon and Heathershaw is based on a coherent structure of turbulence which is one of the most important topics in modern turbulence research.   The simultaneous measurements of the velocity components u and v enables one to investigate coherent structures such as bursting phenomena in both laboratory and field flows.   In the 1980's, a two-component electromagnetic flow meter was considerably miniaturized to improve compactness, sensitivity and stability.   Since such a miniaturized electromagnetic flow meter is not influenced by suspended sediment and water quality, this instrument is now often used in rivers and estuaries, as indicated in Table 1. In this study, three-dimensional turbulence measurements were conducted in an urban

Table 1   Example of turbulence measurements in rivers and estuaries.

Resear-chers	Year	Journal	Instru-ment	Velocity Component	Test Field	Flow Depth h(m)	Aspect Ratio B/h	Re	Results
Grant et al.	1962	JFM vol. 12	Hot-film	u only	Sea-channel Canada	40	36	10^8	Spectrum Kolmogoroff constant C
Yokoshi	1967	Ph. D Kyoto	Propeller	u only	River Japan	2.7	37	4×10^6	Double structure
McQuivey	1973	USGS Paper	Hot-film	u only	River USA	0.9	24	10^6	Turbulence intensity u'
Gordon	1974	Nature vol. 248	Propeller	u and v	Estuary USA	$8 \sim 9$	?	$10^6 \sim 10^7$	Burst in river
Heather-shaw	1974	Nature vol. 248	Electro-magnetic	u and v	Sea England	40	?	10^7	Burst in sea
Griffith et al.	1981	ASCE HY-3	Electro-magnetic	u and v	River USA	2.4	?	10^6	Turbulence intensity u'
West et al.	1986	ASCE HY-3	Electro-magnetic	u and v	Estuary England	$3 \sim 6$	?	3×10^6	u', v', $-\overline{uv}$ Burst rate
Yokoshi et al.	1986	J. Hyd. E JSCE	Electro-magnetic	u and v	Estuary Japan	$2 \sim 6$	> 50	3×10^6	u', v', $-\overline{uv}$ Burst period
Yoshida et al.	1986	J. Phys. E.	LDA	u only	Estuary Japan	$3 \sim 4$	?	10^6	Spectrum
Sera et al.	1988	J. Hyd. E JSCE	Ultra-sonic	u, v and w	River Japan	0.3	32	4×10^4	u', v', w'
Nezu et al.	1991	J. Hyd. E JSCE	Electro-magnetic	u, v and w	River Japan	2.2	8	8×10^5	u', v', w' 2nd Current

river and an irrigation channel by the simultaneous use of two sets of electromagnetic flow meters.

3.   Theory of Turbulence-Driven Secondary Currents in Open Channels

The secondary currents V and W in a straight channel are governed by the following vorticity equation of the streamwise component Ω (e.g., see Einstein & Li, 1958)

$$\underbrace{V\frac{\partial \Omega}{\partial y} + W\frac{\partial \Omega}{\partial z}}_{A} = \underbrace{\frac{\partial^2}{\partial y \partial z}(\overline{v^2} - \overline{w^2})}_{B} + \underbrace{\left(\frac{\partial^2}{\partial z^2} - \frac{\partial^2}{\partial y^2}\right)\overline{vw}}_{C} + \underbrace{v\nabla^2\Omega}_{D} \qquad (1)$$

$$\Omega \equiv \frac{\partial W}{\partial y} - \frac{\partial V}{\partial z} \qquad (2)$$

U, V, and W denote the components of mean velocity; u, v, and w denote the velocity fluctuations in the x–(streamwise), y–(vertical), and z–(spanwise) directions, respectively. The vorticity equation (1) governs the secondary motions exactly, because this equation

does not contain the primary velocity U. The viscous term D is negligible except for regions near the wall. The term A indicates the advection of vorticity, which shows that secondary currents exist. Term B promotes the generation of secondary currents, and term C suppresses it. Nezu & Nakagawa (1984) verified experimentally and Demuren & Rodi (1984) verified numerically that the generation term B and the Reynolds-stress term C are the dominant ones; they have opposite signs and are much larger than the advection term A. Therefore, the difference between the B and C terms drives the secondary motion.

From a review of the previous findings, Nezu & Nakagawa (1992) have recently summarized the origin and mechanism of secondary currents in channel flows, as shown in Figure 1. Anisotropy between $v' \equiv (\overline{v^2})^{1/2}$ and $w' \equiv (\overline{w^2})^{1/2}$ generates the secondary current of Prandtl's *second* kind, i.e., the turbulence-driven one; in contrast, the secondary current of Prandtl's *first* kind is generated by the centrifugal force in a curved channel and this current is, of course, omitted in the present study.
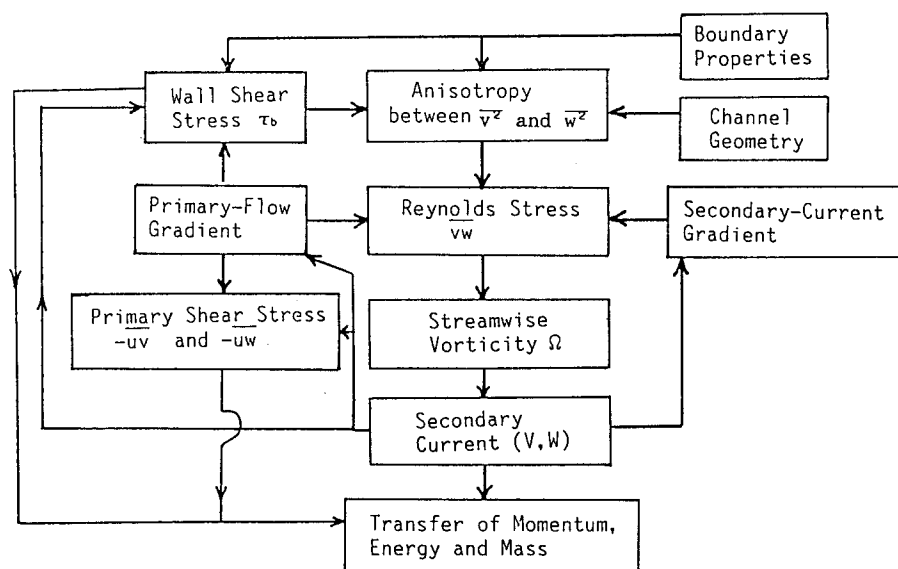

Figure 1   Generation mechanism of secondary currents in channel flows.

In turn, the secondary-current gradient has an important effect on the Reynolds stress $\overline{vw}$. The secondary current also affects the primary flow U, and its velocity gradient affects the wall (bed) shear stress τ_b. Any wavy variation of the bed shear stress along the perimeter will affect the redistribution among three components of the turbulence intensity, u', v' and w'. The primary velocity gradient influences the primary Reynolds stresses $-\overline{uv}$ and $-\overline{uw}$, as can be inferred from the eddy viscosity model. The secondary

currents play an essential role in the lateral transfer of momentum, energy, heat and mass in a channel, and thus their distributions show variations in all three dimensions. Although the mechanism of secondary currents is too complicated to analyze theoretically, the anisotropy between v' and w' is a main cause of their occurrence. Such anisotropy of turbulence is caused in a complex way by boundary conditions at the solid boundaries and the free surface.

Since Prandtl's time, secondary currents of the second kind have been known to occur in non-circular duct flows if the solid-wall effect is strong. These secondary currents are often called "*corner flows*" because they flow from the core toward the corners of duct. Considerable attention has been paid to corner flows in the field of mechanical engineering because many man-made duct flows are non-circular. In contrast, secondary currents in open-channel flows remained comparatively unknown until recently, even though an appearance of secondary currents corresponding to the corner flows of closed channels has been inferred in open channels from observations of the bulging of isovel lines towards the corners. The most important feature associated with such inferred currents is that the maximum velocity appears not at the free surface, but rather just below it in narrow open-channel flows. This phenomenon is called the "*velocity dip*", and it is peculiar to open-channel flows.

Rajaratnam & Muralidhar (1969), Sarma et al. (1983) and the others have inferred from the primary velocity distributions that secondary currents might cause the velocity-dip phenomenon. Low momentum fluids are transported by the secondary motion from the near-bank to the center, and high momentum fluids are moved by this motion from the free surface toward the bed. Kartha & Leutheusser (1970), Knight et al. (1984, 1985) and Nezu et al. (1985) also suggested that wavy distributions of bed shear stress in the spanwise direction are caused by secondary currents. Nezu & Rodi (1985) first conducted accurate measurements of secondary currents in open-channel flows by making use of a high-power LDA system. They found that the effect of the aspect ratio B/h (where, B is the channel width) is significantly pronounced if its ratio is smaller than about 5. Therefore, open-channel flows can be classified into two categories:

i)   Narrow open channels, $B/h \leq 5$.

Corner flows are generated in flows because the side wall produces anisotropy of turbulence in the same manner as for closed-channel flows. In this case, the velocity dip is caused by the free-surface effect whereby the anisotropy of turbulence differs from that for closed-channel flows, as pointed out by Nezu et al. (1989).

ii)   Wide open channels, $B/h > 5$.

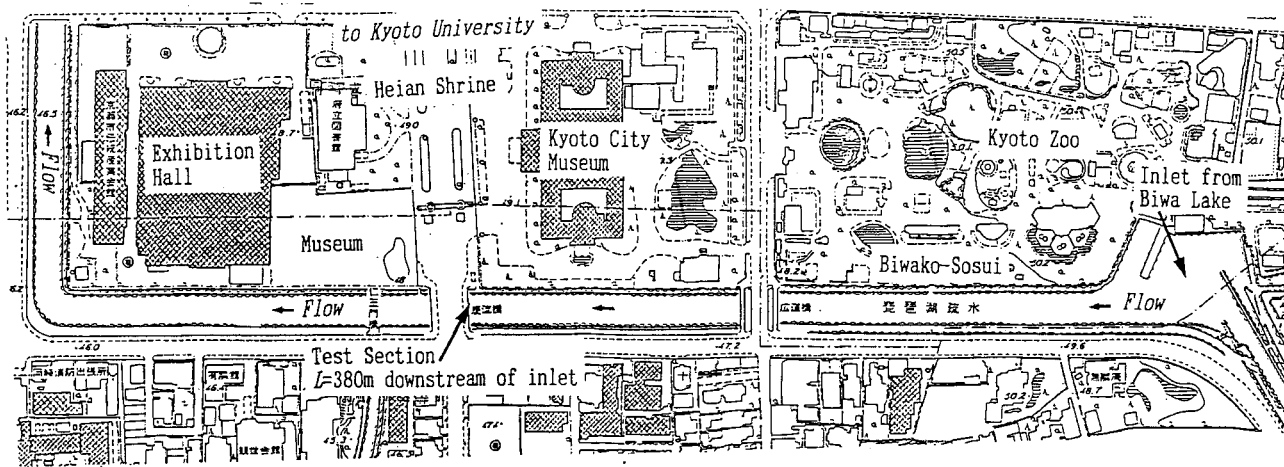In the central zone $|z/h| < (B/h - 5)/2$, the side-wall effect disappears; consequently,

Figure 2   Plane view of the Biwako-Sosui urban river in Kyoto, Japan.
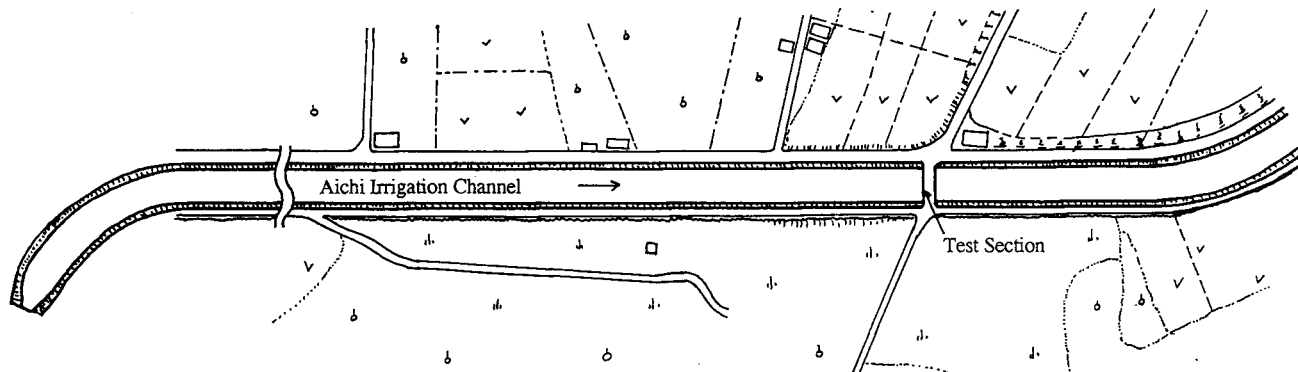

Figure 3   Plane view of the Aichi irrigation channel in Nagoya, Japan.

the 2-D flow properties are attained in the long-term averaged turbulent structures. However, if any spanwise variation of bed shear stress occurs that is periodic, cellular secondary currents and the associated longitudinal bedforms are generated, and vice versa, as pointed out by Nezu & Nakagawa (1989).

4. Field Measurements in Rivers

Figure 2 shows the plane view of the Biwako-Sosui river in Kyoto, which was constructed for water supply more than 100 years ago. The water in this man-made river is introduced from Lake Biwa, the biggest lake in Japan, and it flows through the central zone of Kyoto City. The test section was chosen at a bridge $L = 380$ m downstream from the river inlet; no bridge pier existed upstream of the test section. As indicated in Table 2, the

Table 2   Hydraulic conditions for field measurements.

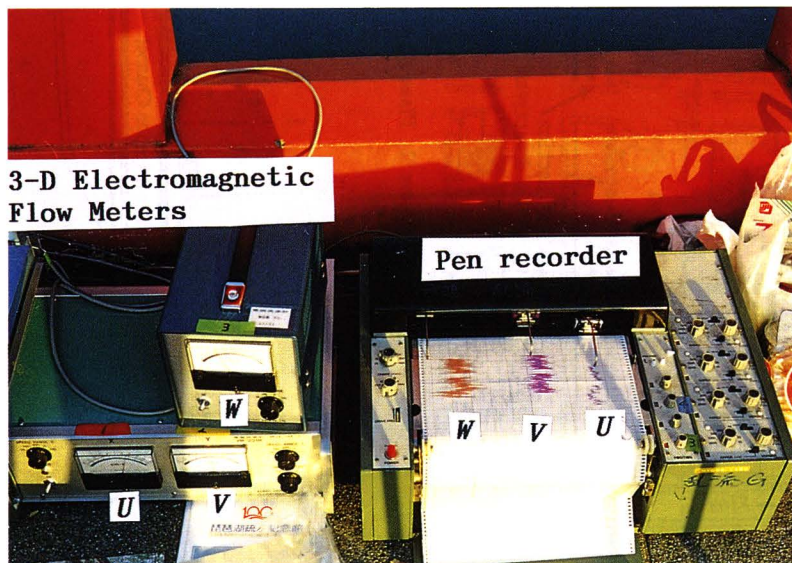|	Flow depth h(m)	Channel Width B(m)	Aspect ratio B/h	Mean velocity U_m(m/s)	Reynolds number Re	Froude number Fr
Biwako Sosui River	2.2	17.5	8.0	0.36	8.0×10^5	0.08
Aichi Irrigation Channel	1.6	4.1	2.5	0.42	6.1×10^5	0.11

Figure 4   Photograph of measurement system.

river width was $B = 17.5$ m, and the flow depth was $h = 2.2$ m.   Therefore, this river can be classified as a "wide" open channel because the aspect ratio B/h is equal to 8.   The cross section of the river was almost rectangular, although some sediment accumulated on the bed.
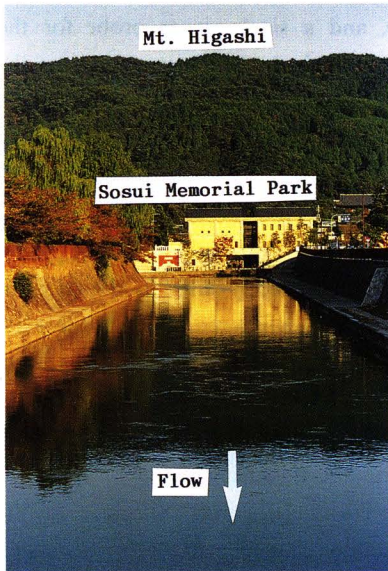
(a)   Measurement location.

(b)   Scene of the upstream from the measurement location.
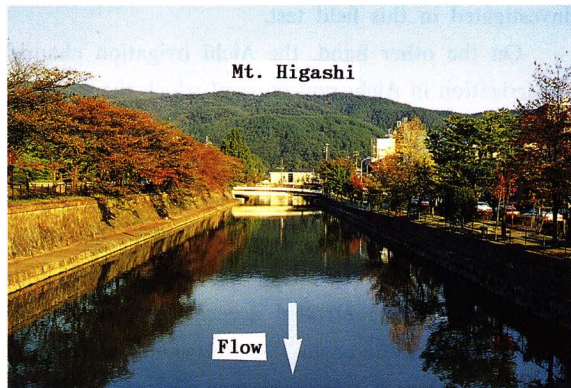
(c)   Enlargement of the photo (b).

(d)   Scene of the downstream from the measurement location.
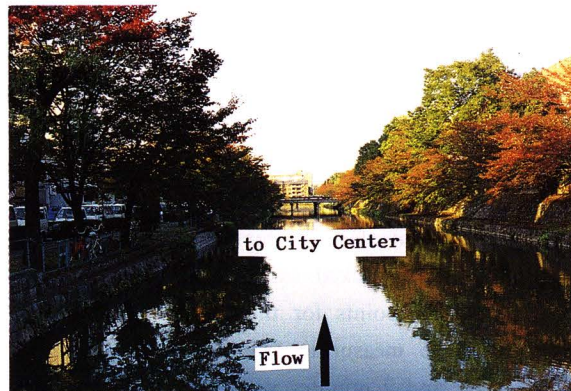

Figure 5   Scene of field measurements of the Sosui river in Kyoto. The lake Biwa is situated behind the Mt. Higashi.

The water discharge was kept constant as $Q = 14\,\mathrm{m}^3/\mathrm{s}$ by a weir at the entrance from the Lake Biwa. Hence, the Reynolds number $Re \equiv U_m h/\nu$ (where, U_m is the mean bulk velocity) became equal to 8×10^5. Since this river, as seen in Figure 2, was a perfectly straight channel with an inlet contracted in the same manner as in a laboratory flume, it was expected that the flow at the test section, $L/h = 173$, was a fully-developed uniform one. Therefore, one may say that the Biwako-Sosui urban river is an ideal counterart of a small-scale laboratory flume and thus that turbulent structures in a large-scale open-channel flow can be investigated in this field test.

On the other hand, the Aichi irrigation channel was constructed about 30 years ago for irrigation in Aichi prefecture of which the capital city is Nagoya. As shown in Figure 3, this channel was also straight for about 250 m distance, and the measurements were conducted at a bridge $L = 200\,\mathrm{m}$ downstream from the beginning of the straight section. The cross section of the channel at the test section was a rectangular one of $B = 4.1\,\mathrm{m}$ wide, and the channel perimeter was covered by flat concrete walls; there was little sediment on the bed because this channel wall was renewed a year before the measurements. The water discharge Q was controlled accurately by a weir; $Q = 2.8\,\mathrm{m}^3/\mathrm{s}$ and $h = 1.6\,\mathrm{m}$ were kept during the measurements. The Reynolds number Re was equal to 6.1×10^5. Therefore, this channel can be classified as a "narrow" open channel because the aspect ratio B/h is equal to 2.5.

In order to measure simultaneously all three components of velocity fluctuations, two sets of electromagnetic flow meters were used in which a dual-sensor probe of 6 mm diameter for the streamwise and vertical components u and v, and a single-sensor probe for the spanwise component w were mounted on a traversing mechanism; the distance between the two probes was set 5.0 cm in order to avoid the electromagnetic interference. As shown in Figure 4, the $u - v$ probe was connected with a two-component electromagnetic flow meter, whereas the w probe was connected with a single-component one. The full scale of the instrument for primary velocity $u(t)$ was 100 cm/s, while that for the secondary velocities $v(t)$ and $w(t)$ was 25 cm/s.

The output signals were recorded on magnetic tapes or floppy discs in digital form with an AD converter. In parallel, the signals of (u, v, w) were monitored by a pen-recorder, and they were checked carefully to avoid abnormal signals. All measuring points were chosen as 270 points for the Biwako-Sosui river and 72 points for the Aichi irrigation channel. The measuring time at a point was 3 minutes with the sampling frequency $f = 100\,\mathrm{Hz}$ and 7 minutes with $f = 40\,\mathrm{Hz}$, depending on the traversing point.

In these field tests, the maximum mainstream velocity $U_{\max}$ was 40.7 cm/s in the Biwako-Sosui river and 55.8 cm/s in the Aichi irrigation channel. A stable traversing mechanism was specially manufactured in order to avoid disturbances due to the Karman vortex and the other vibrations in water flows. Two parallel-connected poles 40 mm in

diameter and 8 m long were fixed on the river bed and at the bridge side, as shown in Figure 5. The rod mounting for the two electromagnetic probes was slid accurately along the parallel poles by a traversing gear.

5. Results and Discussion

5.1 Biwako-Sosui River ($B/h = 8$; wide-channel category)

Figure 6 shows the distributions of primary mean velocity U/U_* versus y/k_s, as a function of the spanwise coordinate z/h, in which k_s is the equivalent sand roughness. The experimental values coincide well with the log-law distribution which is described by

$$\frac{U}{U_*} = \frac{1}{\kappa} \ln\left(\frac{y}{k_s}\right) + A_r \tag{3}$$

where, the Karman constant κ is given as $\kappa = 0.41$ by Nezu & Rodi (1986). A_r is the Nikuradse's integral constant and it is a weak function of the roughness parameter
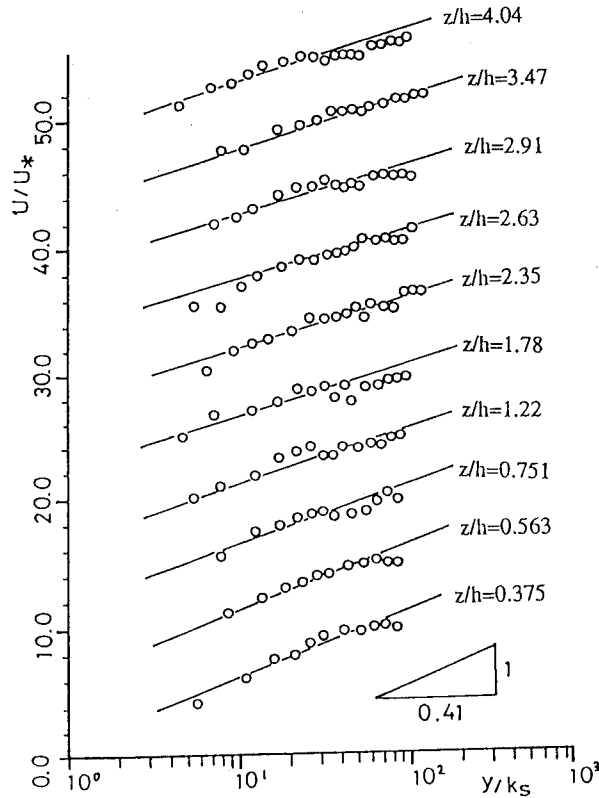

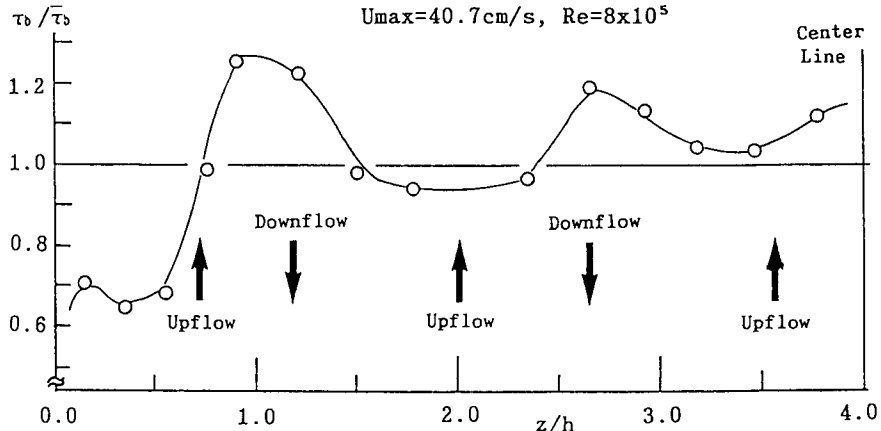Figure 6 Distributions of primary mean velocity, U, in wide river.

Figure 7   Spanwise variation of bed shear stress, τ_b.

$k_s^+ \equiv k_s U_*/\nu$ (e.g., see Tominaga & Nezu, 1992).

Consequently, the local friction velocity $U_*(z)$ could be reasonably evaluated from (3). Figure 7 shows the spanwise variation of bed shear stress $\tau_b \equiv \rho U_*^2$ normalized by its averaged value $\bar{\tau}_b$ along the whole bed. Of particular significance is an undulation of the bed shear stress $\tau_b/\bar{\tau}_b$ in the spanwise direction z/h. As pointed out by Nezu & Nakagawa (1984), the bed shear stress becomes largest at the downflow $(V < 0)$ region of secondary current cell, whereas it becomes smallest at its upflow $(V > 0)$ region. In this manner, the bed shear stress is influenced significantly by the secondary currents, and vice versa, as indicated in Figure 1. This noticeable feature has been observed in both laboratory duct flow by Knight & Patel (1985) and open-channel flow by Nezu & Rodi (1985). This fact was also computer-simulated using the algebraic stress model by Naot & Rodi (1982). The amplitude of the undulation in the bed shear stress is nearly equal to $(0.2-0.3)\bar{\tau}_b$, although it tends to decrease farther from the bank. This undulation of the bed shear stress is very important in considering various mass transports such as sediment and water quality in rivers.

Figure 8 shows the isovel lines of the primary mean velocity $U(y, z)$ in a half section of the river. The isovel lines undulate considerably in the spanwise direction, and thus the turbulent structure is evidently three-dimensional throughout the cross section of river. However, the maximum velocity did not appear below the free surface, but on the free surface. The present field measurements confirm that no velocity-dip phenomena occur because the aspect ratio B/h is greater than 5. The isovel lines bulge toward the free surface at about $z/h = 1.9$ and 3.7, and thus form the low-speed zones near the free surface; these correspond well to the regions of upflows and low bed shear stress that are shown in Figure 7. On the other hand, the isovel lines bulge toward the bed at about $z/h = 1.3$ and 2.6, and thus form the high-speed zones, which correspond to the regions of downflows and high bed

Figure 8   Isovel lines of primary velocity, $U(y, z)$.

shear stress.   Therefore, the spanwise spacing ℓ between the low-speed zones at the free surface is nearly equal to $1.8\,h$.   This value is slightly smaller than the well-known relation of $\ell = 2\,h$ observed by Kinoshita (1967) in sufficiently wide rivers with $B/h \simeq 100$.   This smaller value may have been caused by the stronger restraint due to the relatively small aspect ratio, i.e., $B/h = 8$.

Figure 9 shows the contour lines of the vertical velocity $V(y, z)$.   Figure 10 shows the vector description of secondary currents (V, W) which were measured by the simultaneous use

Figure 9   Contour lines of vertical secondary velocity, $V(y, z)$.

Figure 10   Vector description of secondary currents (V, W).

of two sets of electromagnetic flow meters. Since no correction was made in the raw data measured directly by the different electromagnetic flow meters, the plotted values may have included experimental errors considerably due to the instrument accuracy, but they evidently show multi-pairs of the upflow ($V > 0$) and downflow ($V < 0$) in the cross section. Such a pair of the upflow and downflow of secondary currents corresponds well to the undulation property of the primary velocity and the bed shear stress shown in Figures 7 and 8. The maximum value of the secondary currents is below 4 % of the maximum primary velocity U_{max}. These field observations coincide well with the accurate LDA data in laboratory flumes, e.g., see Nezu & Nakagawa (1992). Of particular significance is evidence of the appearance of cellular secondary currents in an actual river, as indicated by handwriting in Figure. 10. The spanwise size of a pair of these cellular currents is about $\ell = 1.8\,h$ for the aspect ratio $B/h = 8$. A strong secondary current may be recognized near the bed close to the river bank. Since some sediment accumulated on the bed close to the bank as shown in Figure 10, the secondary currents might have been affected significantly by these sediments.

Figure 11 shows the contour lines of turbulence intensities u' and v' that were normalized by U_{max}. Evidently, the turbulence structure indicates three-dimensional patterns that undulate considerably in the spanwise direction owing to the secondary-current motions, and vice versa. It can be recognized from Figure 11 that the turbulence intensity becomes higher at the upflow region, whereas it becomes lower at the downflow region. The most
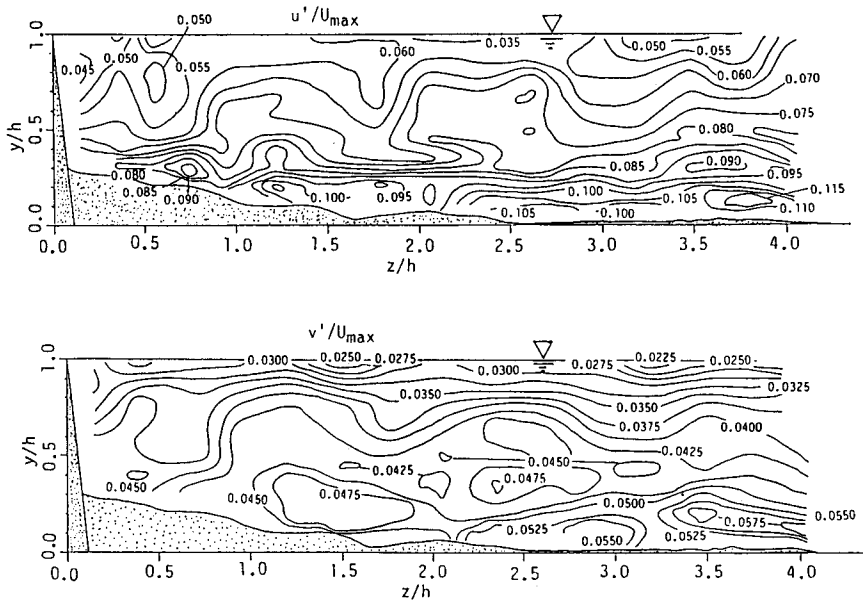

Figure 11   Contour lines of turbulence intensities, u' and v'.

important feature is that the vertical turbulence intensity v' is much more depressed near the free surface than the horizontal components u' and w'; anisotropy of turbulence becomes much stronger near the free surface as compared with duct flows.   These features of river turbulence are in a good agreement with laboratory data.

5.2   Aichi Irrigation Channel ($B/h = 2.5$; narrow-channel category)

The main results of the field measurements conducted in the Aichi irrigation channel were compared with the accurate LDA data in the laboratory flumes obtained by Nezu *et al.* (1989) and also with the computer simulation calculated by Naot & Rodi (1982); the aspect ratio of the latter two was both equal to 2.

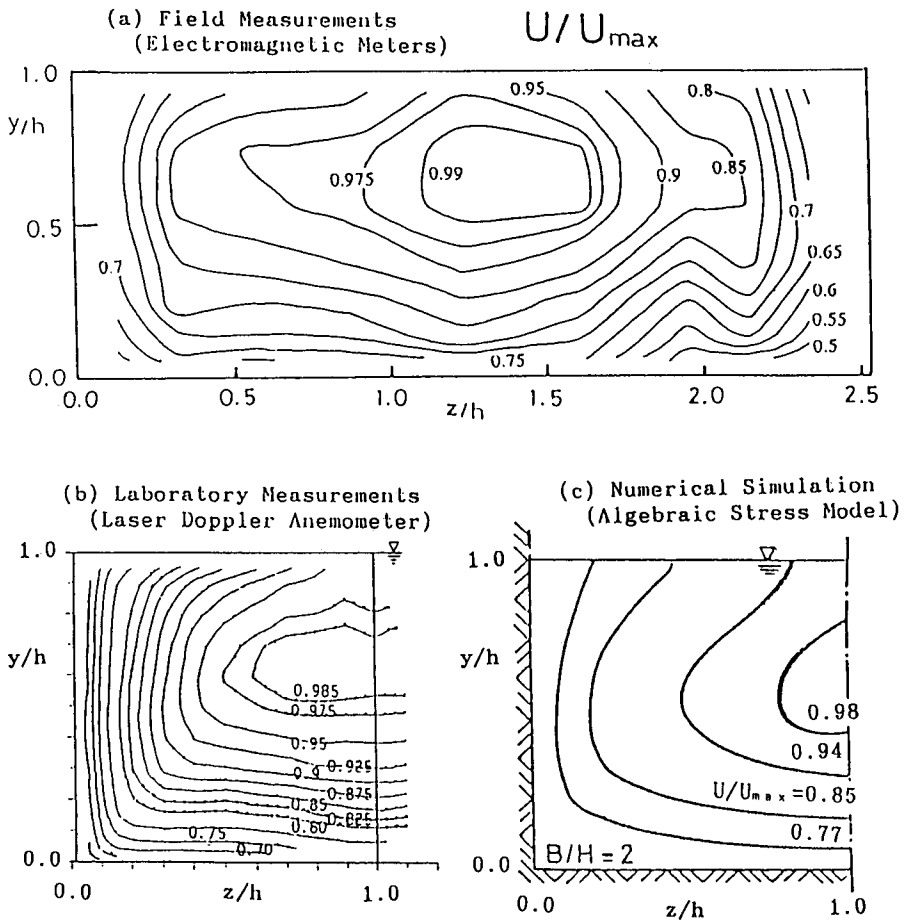Figure 12 shows the isovel lines of primary mean velocity $U(y, z)$ for (a) field channel,

Figure 12   Comparison of isovel lines of primary velocity for (a) field channel, (b) laboratory flume and (c) numerical simulation.

(b) laboratory flume and (c) computer simulation; the former shows the whole cross section of channel, whereas the latter two show the half cross section. Of particular significance is that the maximum velocity is evident below the free surface, in contrast with the case of the Biwako-Sosui river shown in Figure 8. This fact also confirms that the velocity-dip phenomenon does occur when the aspect ratio is smaller than 5. The elevation of the maximum velocity for the field channel was about $y/h = 0.6 - 0.7$, which coincides well with the laboratory data and also with the computer simulation.

Figure 13 compares the stream lines ψ for (a) field channel, (b) laboratory flume and (c) computer simulation. The stream function ψ could be calculated using the measured values of W, as follows:
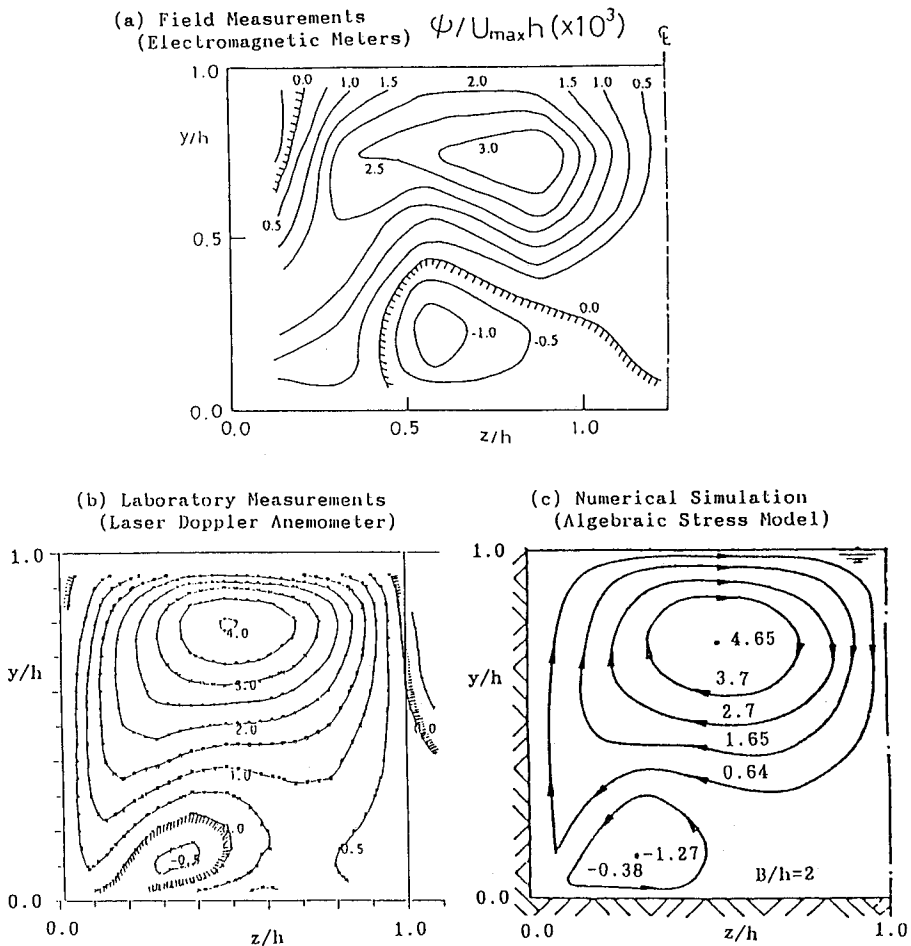
Figure 13 Comparison of streamlines $\psi(y, z)$ of secondary currents for (a) field channel,
(b) laboratory flume and (c) numerical simulation.

$$\psi = -\int_0^y W dy \qquad (4)$$

It should be noted that the free-surface vortex and the bottom vortex are observed clearly in the irrigation channel; the former vortex is much larger than the latter. The structure of such secondary currents observed in the field stream is quite consistent with that measured in laboratory flumes and also with the numerical calculations. These facts imply that the mechanism of turbulence-driven secondary currents is the same in both the field stream and laboratory flume; this mechanism can be explained well by the vorticity equation (1).

Figure 14 shows the distributions of primary mean velocity U/U_* against the vertical coordinate y/k_s. Although the measuring points in the Aichi irrigation channel were much smaller than those in the Biwako-Sosui river shown in Figure 6, the experimental values of U coincide well with the log-law distribution of (3) in the wall region; the velocity-dip phenomenon is seen clearly in the outer region in Figure 14.
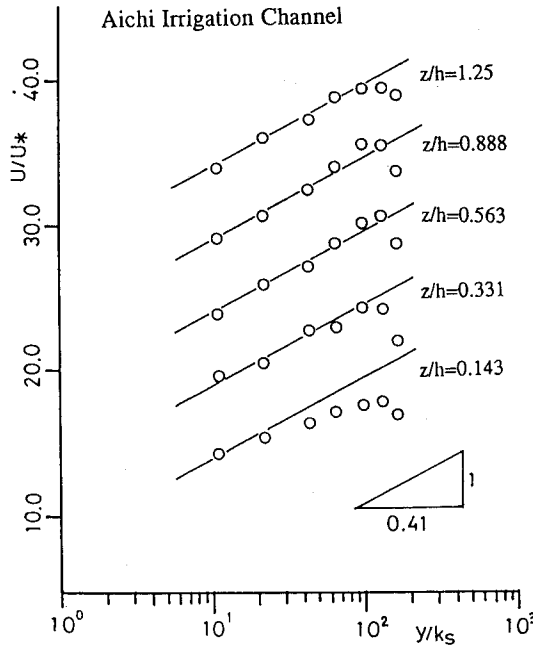

Figure 14   Distributions of primary mean velocity, U, in narrow river.

Therefore, the local friction velocity $U_*(z)$ could be evaluated reasonably from this log-law distribution in the same manner as in Figure 6. The equivalent sand roughness k_s in this field channel was nearly equal to 9.2 mm, and thus $k_s^+ \equiv U_* k_s/v$ became about 220, which belongs to a completely rough regime, i.e., $k_s^+ > 70$. Figure 15 shows the spanwise
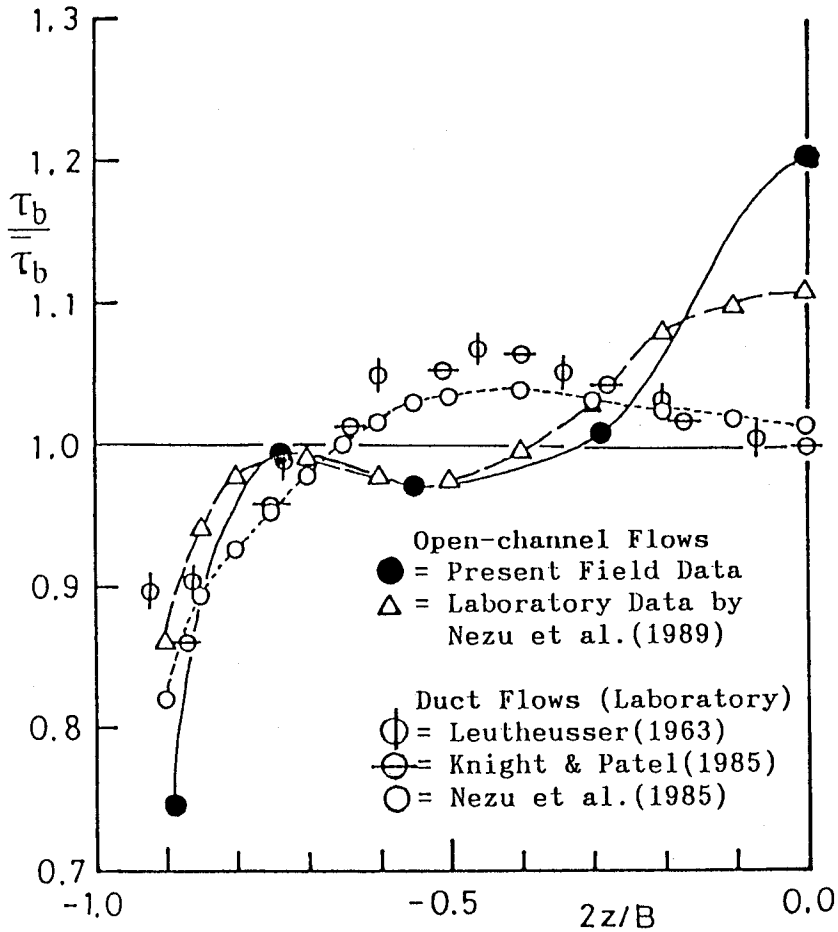
Figure 15   Comparison of bed shear stress distribution in duct and open-channel flows.

variation of the bed shear stress $\tau_b = \rho U_*^2$ in the field stream.   For comparison, this figure contains the laboratory data that were obtained for open-channel flows by Nezu *et al.* (1989) and also for duct flows by Leutheusser (1963), Knight & Patel (1985) and Nezu *et al.* (1985).   The present field data of τ_b coincide well with the laboratory ones in open-channel flows.   The amplitude of this spanwise undulation for the narrow channel is the nearly same as that for the wide river shown in Figure 7.

Of particular significance is the considerable difference between the bed shear stress distributions for ducts and open channels.   For open-channel flow, the value of τ_b increases rapidly with distance from the side wall, and it shows a mild peak followed by a valley at $z/(B/2) \simeq \pm 0.5$.   Beyond this position, it increases again, and attains a maximum at the central axis.   In contrast, the bed shear stress for duct flow is a minimum at the central
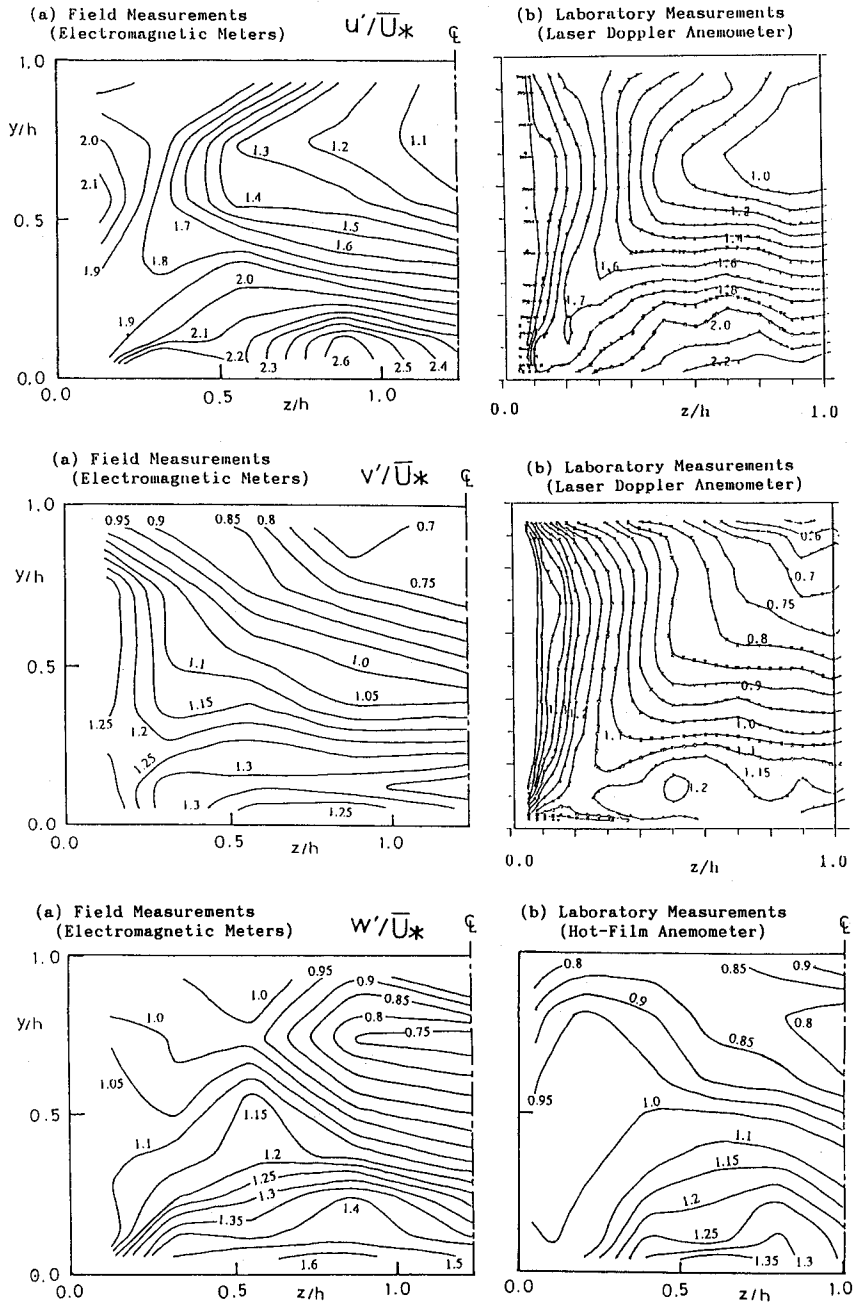
Figure 16   All three components of turbulence intensity, u', v' and w', for (a) field channel and (b) laboratory flume.

axis. Consequently, the spanwise variation of bed shear stress for duct flows is out of phase with that for open-channel flows. Such an important difference of bed shear stress in duct and open-channel flows is due to the essential difference of the corresponding secondary currents, as pointed out by Nezu et al. (1989).

Figure 16 shows contour lines of all three components of turbulence intensity, u', v', and w', for (a) field channel and (b) laboratory flume. These values are normalized by the friction velocity $\bar{U}_*$ averaged along the perimeter. The values of u' and v' in a laboratory flume were measured with an LDA system by Nezu & Rodi (1985). However, the corresponding value of w' was measured with a refined hot-film system by Tominaga et al. (1989) because it was impossible to measure the w' component with an LDA. The present field channel was completely rough, whereas the laboratory flume was hydraulically smooth. The 3-D structures of all three components of turbulence intensity in both the field data and laboratory data are quite similar. The horizontal components, u' and w', both indicate minimum values not at the free surface, but just below it; this corresponds well to the velocity-dip phenomenon shown in Figure 12. In contrast, the vertical component, v', decreases monotonously as the free surface is approached; this special damping of v' is caused by the existence of free surface, as discussed in detail by Nezu & Nakagawa (1992). Therefore, it can be concluded that the anisotropy of turbulence intensity among u', v' and w' becomes much stronger near the free surface in both field and laboratory open channels than in the corresponding closed ducts.

6. Generation Mechanism of Longitudinal Vorticity

Nezu & Nakagawa (1984) verified that the term $B \equiv \partial^2(\overline{w^2} - \overline{v^2})/\partial y \partial z$ in equation (1) is the dominant generation term of the longitudinal vorticity, Ω, and they then predicted that cellular secondary currents rotate clockwise at $B < 0$, whereas these currents rotate counterclockwise at $B > 0$. Figure 17 shows the contour lines of $(\overline{w^2} - \overline{v^2})/\bar{U}_*^2$ that were directly measured with the use of an electromagnetic flow meter in the Biwako-Sosui
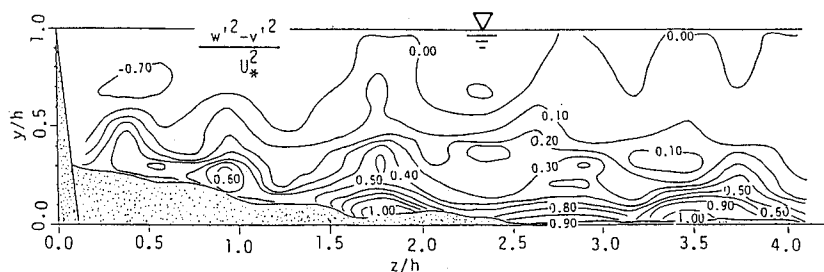

Figure 17   Contour lines of vorticity production term in a wide river.

river. These contours show a wavy cyclic pattern in the spanwise direction, and thus the term B never becomes zero constant even farther from the bank. Evidently, the characteristics of the term B can explain reasonably an appearance of cellular secondary currents in a wide river.

In the case of narrow open channels such as the Aichi irrigation channel, terbulence intensities are significantly affected by both the free surface and the side walls. Figure 18 shows the contour lines of $(\overline{w^2} - \overline{v^2})/\overline{U}_*^2$, together with the laboratory data obtained by Tominaga *et al.* (1989). Although the values of $(\overline{w^2} - \overline{v^2})/\overline{U}_*^2$ were slightly different between the field channel and the laboratory flume, these overall structures are almost the same in both measurements. The values of $(\overline{w^2} - \overline{v^2})$ become negative near the side walls and they become larger as the free surface is approached. Nezu *et al.* (1989) and Tominaga *et al.* (1989) have verified that such distorted distributions of $(\overline{w^2} - \overline{v^2})$ in open channels cause the characteristic structure of secondary currents which is quite different from that in closed ducts. Consequently, the generation mechanism of these secondary currents peculiar to open-channel flows can be applied to field channels in which the Reynolds number is by one order or more larger than in laboratory channels.
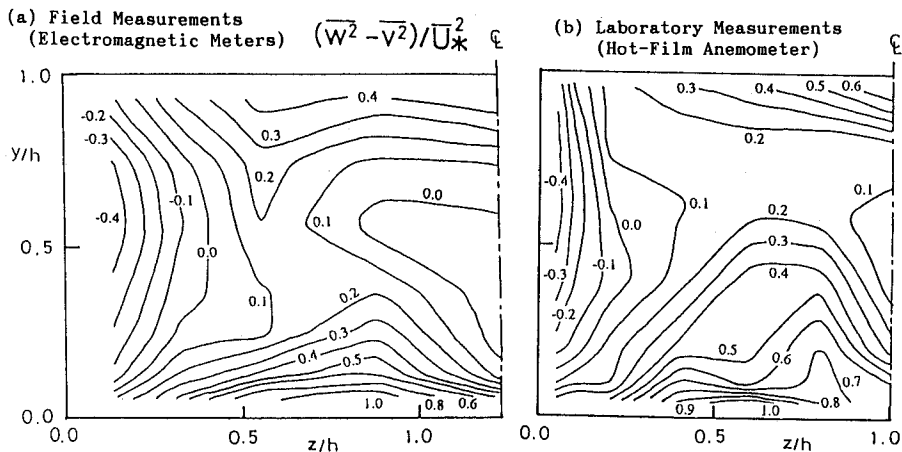

Figure 18 Contour lines of vorticity production term in narrow channels for (a) field and (b) laboratory.

7. Conclusions

In this study, field measurements of turbulence in both the Biwako-Sosui urban river at Re = 8 × 10⁵ in Kyoto and the Aichi irrigation channel at Re = 6 × 10⁵ in Nagoya have been conducted using specially designed three-component electromagnetic flow meters. The former waterway belongs to the wide-channel category, the latter to the narrow-channel

category. The present field tests first found that multi-cellular secondary currents were evident in a wide river and also that free-surface secondary currents associated with the velocity-dip phenomenon appeared in a narrow river, in which the Reynold numbers were by one order or more larger than that of laboratory flows.

It was verified theoretically and experimentally that these secondary currents are generated by anisotropy of turbulence, i.e., the term of ($\overline{w^2} - \overline{v^2}$). These currents significantly influence the patterns of primary mean velocity, bed shear stress and various turbulence characteristics in the whole cross section of rivers. From comparisons between the field data and the laboratory data, it can be concluded that three-dimensional turbulent structures associated with secondary currents are almost universally, independent of the Reynolds numbers. Therefore, the accurate laboratory data of open-channel turbulence measured with a laser-Doppler anemometer can be applied to river turbulence at high Reynolds numbers.

The spanwise undulations of primary velocity and bed shear stress are essential properties in considering various transport phenomena of momentum, heat and mass such as suspended sediment and water quality in rivers and estuaries. It is further necessary to develop a refined turbulence model in order to predict these complicated 3-D turbulent structures and the associated transport phenomena in rivers and estuaries.

Acknowledgement

References

Allen, J. R. L. (1985): *Principles of physical sedimentology*, George Allen & Unwin, Chapter 11.

Culbertson, J. K. (1967): Evidence of secondary circulation in an alluvial channel, U. S. Geol. Survey, Prof. Paper 575-D, pp. 214–216.

Demuren, A. O. and Rodi, W. (1984): Calculation of turbulence-driven secondary motion in non-circular ducts, J. Fluid Mech., Vol. 140, pp. 189–222.

Einstein, H. A. and Li, H. (1958): Secondary currents in straight channels, Trans. Amer, Geophys. Union, vol. 39, pp. 1085–1088.

Gibson, A. H. (1909): On the depression of the filament of maximum velocity in a stream flowing through an open channel, Proc., Royal Soc. of London, Series A, vol. 82, pp. 149–159.

Gordon, C. M. (1974): Intermittent momentum transport in a geophysical boundary layer, Nature, vol. 248, pp. 392–394.

Grant, H. L., Steward, R. W. and Moilliet, A. (1962): Turbulent spectra from a tidal channel, J. Fluid Mech., vol. 12, pp. 241–268.

Heathershaw, A. D. (1974): "Bursting" phenomena in the sea, Nature, vol. 248, pp. 394–395.

Karcz, I. (1966): Secondary currents and the configuration of a natural stream bed, J. Geophys.

Research, vol. **71**, pp. 3109–3116.

Kartha, V. C. and Leutheusser, H. J. (1970): Distribution of tractive force in open channels, J. Hydraulics Div., ASCE, vol. **96**, HY-7, pp. 1469–1483.

Kinoshita, R. (1967): An analysis of the movement of flood waters by aerial photography; Concerning characteristics of turbulence and surface flow, Photographic Surveying, vol. **6**, pp. 1–17 (in Japanese).

Knight, D. W., Demetriou, J. D. and Hamed, M. E. (1984): Boundary shear in smooth rectangular channels, J. Hydraulic Eng., ASCE, vol. **110**, pp. 405–422.

Knight, D. W. and Patel, H. S. (1985): Boundary shear in smooth rectangular ducts, J. Hydraulic Eng., ASCE, vol. **111**, pp. 29–47.

Leutheusser, H. J. (1963): Turbulent flow in rectangular ducts, J. Hydraulics Div., ASCE, vol. **89**, HY-3, pp. 1–19.

Möller, M. (1883): Studien über die Bewegung des Wassers in Flüssen mit Bezugnahme auf die Ausbildung des Flussprofiles, Zeitsharift für Bauwesen, p. 201, (A summary in English is given in *Hydraulic Laboratory Practice*, edied by J. R. Freeman, ASME, 1929, p. 70).

Naot, D. and Rodi, W. (1982): Calculation of secondary currents in channel flow, J. Hydraulics Div., ASCE, vol. **108**, pp. 948–968.

Nezu, I. and Nakagawa, H. (1984): Cellular secondary currents in straight conduit, J. Hydraulic Eng., ASCE, vol. **110**, pp. 173–193.

Nezu, I. and Nakagawa, H. (1989): Self forming mechanism of longitudinal sand ridges and troughs in fluvial open-channel flows, Proc. of 23 rd IAHR Congress, Ottawa, vol. **B**, pp. 65–72.

Nezu, I. and Nakagawa, H. (1992): *Turbulence in Open-Channel Flows*, IAHR-monograph, Balkema Publishers, Rotterdam (in printing).

Nezu, I., Nakagawa, H. and Rodi, W. (1989): Significant difference of secondary currents in closed channels and narrow open channels, Proc. of 23 rd IAHR Congress, Ottawa, vol. **A**, pp. 125–132.

Nezu, I., Nakagawa, H. and Tominaga, A. (1985): Secondary currents in a straight channel flow and the relation to its aspect ratio, *Turbulent Shear Flows* 4, Springer-Verlag, vol. **4**, pp. 246–260.

Nezu, I. and Rodi, W. (1985): Experimental study on secondary currents in open channel flow, Proc of 21 st Congress of IAHR, Melbourne, vol. **2**, pp. 115–119.

Nezu, I. and Rodi, W. (1986): Open-channel flow measurements with a Laser Doppler anemometer, J. Hydraulic Eng., ASCE, vol. **112**, pp. 335–355.

Rajaratnam, N. and Muralidhar, D. (1969): Boundary shear stress distribution in rectangular open channels, La Houille Blanche, No. **6**, pp. 603–609.

Sarma, K. V. N., Lakshminarayana, P. and Rao, N. S. L. (1983): Velocity distribution in smooth rectangular open channels, J. Hydraulic Eng., ASCE, vol. **109**, pp. 270–289.

Stearns, F. P. (1883): On the current meter, together with a reason why the maximum velocity of water flowing in open channels in below the surface, Trans. of ASCE, vol. **12**, No. 216, pp. 331–338.

Tominaga, A. and Nezu, I. (1992): Velocity profiles in steep open-channel flows, J. Hydraulic Eng., ASCE, vol. **118**, No. 1, pp. 73–90.

Tominaga, A., Nezu, I., Ezaki, K. and Nakagawa, H. (1989): Three-dimensional turbulent structure in straight open-channel flows, J. Hydraulic Research, IAHR, vol. **27**, pp. 149–173.

Vanoni, V. A. (1946): Transportation of suspended sediment by water, Trans. of ASCE, vol. **111**, pp. 67–133.